2026 IEEE International Conference on Robotics and Automation (ICRA 2026)
June 1-5, 2026. Vienna, Austria

Electrospun TPU/LCE Composite Fibers for High-Performance Biomimetic Tendon Actuation

Yongzheng Luo, Shen Gao, Mingjun Tang, Yue Wang*, Tao Yue *Member, IEEE*

***Abstract*—Traditional rigid actuators in soft robotics, particularly for bionic hands, suffer from structural complexity, bulkiness, and limited biomimetic motion. To address these limitations, we developed an electrospun composite fiber membrane composed of thermoplastic polyurethane (TPU) and liquid crystal elastomer (LCE), and demonstrated its feasibility as a tendon-like soft actuator in an artificial finger. TPU provides elasticity and mechanical robustness, while LCE contributes reversible thermal contraction as the actuation unit. The resulting TPU-LCE fibers exhibit high flexibility comparable to biological muscle and outstanding actuation performance. Under thermal stimulation, the actuator achieved a contraction strain of up to 44.4% and a load-bearing capacity exceeding 3,500 times its own weight, while maintaining durability over 120 actuation cycles without significant degradation. Integrated into a tendon-driven biomimetic finger, the actuator enabled smooth and natural joint motions, closely resembling human finger flexion–extension gestures. This work presents a reliable and scalable bio-inspired actuation strategy, offering promising potential for soft robotics applications.**

I. Introduction

Traditional rigid actuators—such as electric motors or combustion engines—are inherently limited in safety, efficiency, and miniaturization due to their rigidity and structural complexity. As the scale decreases, manufacturing costs and technical challenges rise even further. In contrast, biological muscle represents a natural soft actuator with remarkable efficiency, reversibility, and adaptability, operating through ATP-driven contraction [1–3]. Inspired by this performance, researchers have pursued soft actuators based on engineered responsive materials, capable of reversible contraction, expansion, and bending, and able to mimic biological functions.

Among these materials, liquid crystal elastomers (LCEs) have emerged as promising artificial muscle candidates because they combine the molecular anisotropy of liquid crystals with the elasticity of cross-linked polymer networks, enabling large reversible strain and programmable deformation [4–9]. Proper alignment of mesogens into monodomain structures is key to achieving such actuation [10,11]. Recent advances include bio-inspired spinning of highly aligned LCE microfibers with rapid and durable actuation [12], as well as ultrathin gold-coated LCE films achieving electrically controlled contraction via Joule heating [13]. These studies highlight the potential of LCEs, yet fiber-based actuators remain limited by brittleness, reduced toughness, and insufficient load capacity.

Various composite strategies have been developed to enhance performance, for example combining LCEs with stretchable thermoelectrics [14] or carbon nanotubes [15]. While these approaches introduce functionalities such as electrical control or photothermal response, they often compromise toughness or fail to achieve large-amplitude axial contraction. Current LCE fiber fabrication methods—including melt, wet, dry, and electrospinning techniques—still face trade-offs between strain, response speed, and force output [16,17]. Notably, electrospinning, though well-established for polymers, has seldom been systematically applied to LCE fibers.

This study addresses these challenges by introducing a composite electrospinning route that integrates thermoplastic polyurethane (TPU) with LCE. TPU contributes elasticity, mechanical strength, and fracture toughness, counteracting the intrinsic brittleness of pure LCE, while retaining its actuation behavior [18,19]. Using optimized electrospinning parameters, followed by mechanical stretching and UV curing, we achieve uniaxially aligned TPU–LCE composite fibers with stable thermal responsiveness.

We further demonstrate their application as artificial tendons in a tendon-driven biomimetic finger device. Inspired by the skeleton–tendon architecture of human fingers, TPU–LCE fibers are embedded into a 3D-printed framework as flexor and extensor tendons, enabling smooth and natural joint actuation (Fig. 1a &1b) . Experimental results validate that the proposed actuator achieves biomimetic performance while maintaining robustness and scalability.

The key contributions of this work are:

1) Developing a stable electrospinning process for TPU–LCE composite fibers with uniaxial orientation.

2) Demonstrating high thermal actuation performance—44.4% contraction strain, load capacity >3,500× self-weight, and stable cyclic operation over 120 cycles.

3) Implementing the fibers in a tendon-driven biomimetic finger, achieving human-like joint motion with smooth bidirectional actuation.

This work was supported by the grants from the National Natural Science Foundation of China (No. 62303290).

(Yongzheng Luo, Shen Gao, Mingjun Tang, Yue Wang) School of Future Technology, Shanghai University, Shanghai, China (e-mail: luoyongzheng@shu.edu.cn, gaoshen@shu.edu.cn, tmj@shu.edu.cn, yue_wang@shu.edu.cn)

(Shen Gao, Tao Yue) School of Mechatronic Engineering and Automation, Shanghai University, Shanghai, China (e-mail: tao_yue@shu.edu.cn)

*Corresponding author

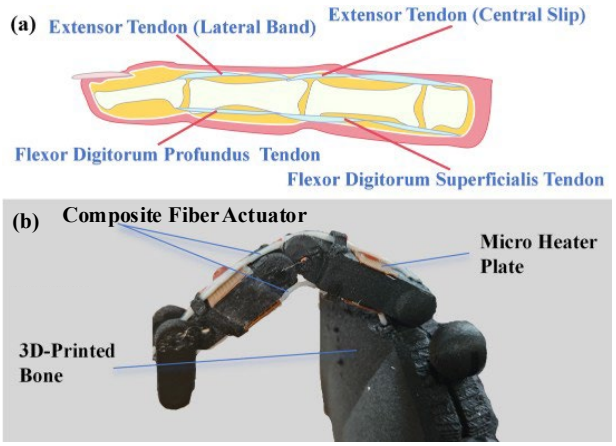

Figure 1. (a) Anatomical reference of the human finger tendon and bone distribution. (b) Schematic of the tendon-driven biomimetic finger device, showing the 3D-printed skeleton and integrated artificial tendons.

II. Materials Processing and Manufacturing

A. Preparation of Electrospinning Ink

To formulate the TPU–LCE spinning ink, the following components were used: liquid crystal monomer 1,4-bis-[4-(3-acryloyloxyhexyloxy)benzoyloxy]-2-methylbenzene (RM257), thermoplastic polyurethane elastomer (TPU), photoinitiator diphenyl(2,4,6-trimethylbenzoyl) phosphine oxide (TPO), dithiol chain extender 2,2′-(ethylenedioxy)diethanethiol (EDDET), tetrathiol crosslinker pentaerythritol tetrakis(3-mercaptopropionate) (PETMP), inhibitor 2,6-di-tert-butyl-4-methylphenol (BHT), and catalyst dipropylamine (DPA).

First, 4 g of RM257 was dissolved in a 1:1 mixture of DMF and acetone, followed by the dropwise addition of 0.51 g PETMP, 667 µL EDDET, and 8 µL DPA catalyst. The system was stirred for 8 hours under light-proof conditions to complete the pre-crosslinking treatment (Fig. 2a). The primary reason for pre-crosslinking is that experimental observations revealed that directly injecting uncrosslinked LCE ink into the electrospinning nozzle resulted in insufficient initial viscoelasticity and spinnability, preventing the formation of continuous and stable fibers, often leading to droplet precipitation or filament breakage. Therefore, inducing a certain degree of pre-crosslinking via thiol-ene click reaction enhances the modulus and cohesive strength of the ink, significantly improving fiber-forming performance during the spinning process. After pre-crosslinking, 0.64 g TPU (16% by mass of RM257) was dissolved in DMF solvent at 65 °C, and this solution was thoroughly mixed with the aforementioned LCE ink.

Finally, the mixture was vacuum-degassed, and 0.05 g TPO photoinitiator and 0.03 g BHT were added. TPO is intended for subsequent UV-induced curing and crosslinking, while BHT acts as a polymerization inhibitor to prevent premature progression of the thiol-ene click reaction during spinning, avoiding clogging of the nozzle due to crosslinking. All chemicals were used as received without further purification: RM257 (Bidepharm, 95%), PETMP/EDDET (Macklin, 98%), acetone (Sinopharm Chemical Reagent, 99%), DMF/DPA (Aladdin, 95%).

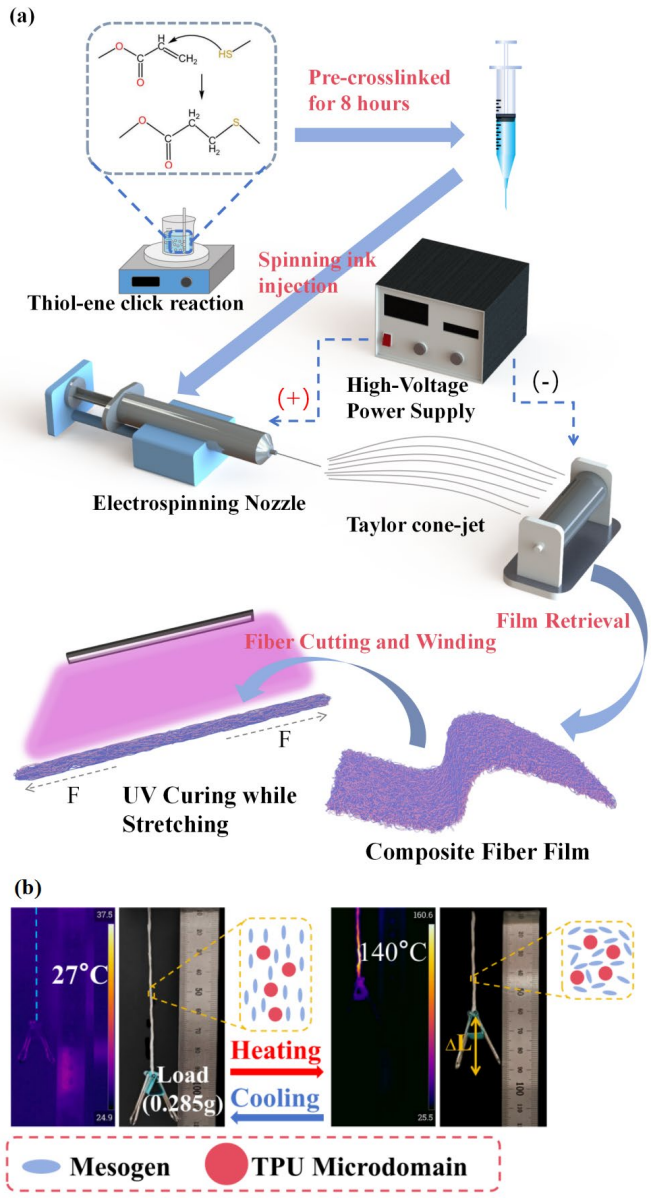

Figure 2. (a) Schematic of the entire fabrication process of the TPU-LCE composite fiber, from ink preparation to electrospinning. (b) Physical actuation mechanism and corresponding thermodynamic behavior of the TPU-LCE fiber upon thermal stimulation.

B. Electrospinning Parameters Configuration

The configuration of electrospinning parameters plays a decisive role in the final forming quality of the fibers. Among the processing parameters, the voltage directly affects the electric field intensity: an increase in voltage enhances the electric field force, resulting in more significant jet acceleration and greater stretching degree, which helps reduce fiber diameter; however, excessively high voltage can easily lead to jet instability, severe whipping, and an expanded deposition area on the collector. The ink flow rate is a critical factor affecting the occurrence of bead formation and fiber adhesion in the fiber membrane; moreover, the flow rate must be coordinately matched with the voltage parameter. The setting of the collection distance requires comprehensive consideration of the solvent's volatility and the chemical properties of the solute. Environmental parameters represent

another important category of regulatory factors. To ensure sufficient solvent evaporation during the jetting process, the ambient humidity should be maintained within a certain range. Simultaneously, the ambient temperature also influences the solvent evaporation rate and further affects the fiber's microscopic morphology by modulating the solution viscosity. Based on the above considerations, electrospinning was conducted in this experiment using a 21-gauge nozzle and a collector rotating at 1500 rpm, under an environment with a constant temperature of 40 °C and a relative humidity of 30 ± 5%. The experimental parameters were set as follows: an applied voltage of 25 kV, a distance of 20 cm between the nozzle and the collector, and an advancing rate of 5 milliliters per hour (mL/h) (Table I). These parameters were carefully optimized: the voltage ensures stable jetting to form a whip-free structure; the distance controls the sufficient volatilization of the solvent; and the flow rate balances continuity and morphological regulation. The set rotation speed of the collector can promote the fracture-free aligned arrangement of fibers, while the controlled temperature and humidity range effectively reduces bead defects. Finally, uniform fibers with a diameter of 10–40 μm were obtained, which possess both structural stability and efficient thermoresponsive properties.

TABLE I. ELECTROSPINNING PARAMETERS FOR TPU-LCE COMPOSITE FIBER FABRICATION

Parameter	*Value/Setting*	*Unit*
Applied Voltage	+25	kV
Working Distance	20	cm
Flow Rate	5	mL/h
Nozzle Gauge	21	G
Rotational Speed	1500	rpm
Ambient Temperature	40	°C
Ambient Humidity	30 ± 5	% RH

From Fig. 3a, it can be observed that the electrospun TPU–LCE mat forms a non-woven, porous fibrous network resembling a spider's web in macroscopic morphology. The diameter of these fibers ranges from 10 to 40 μm, which is comparable to that of natural tendon fibers, thereby enhancing the bionic relevance of the composite. Due to the use of a high-speed rotating drum collector, the ultrafine fibers exhibit preliminary alignment along the collection direction. However, without any post-treatment (e.g., mechanical stretching or surface alignment), the as-prepared TPU–LCE samples typically display a multi-domain structure with irregular director orientation. Unlike mono-domain LCEs, such multi-domain LCEs behave like conventional elastomers—exhibiting soft elasticity under stretch but lacking stable, reversible actuation strain in response to thermal stimuli.Currently, the most commonly used alignment strategy is to achieve uniaxial orientation in LCEs through mechanical stretching prior to their cross-linking, an approach first proposed by Finkelmann et al [15]. In this work, we draw on this concept by applying mechanical stretching with UV light curing to achieve uniaxial orientation alignment in TPU-LCEs. UV light curing requires a continuous treatment duration of three hours to ensure complete cross-linking of the network. A shorter exposure time will result in insufficient rigidity and unstable actuation, while an excessively long curing time will reduce the deformation capacity due to over-cross-linking. As observed from the differential scanning calorimetry (DSC) curve of the composite fiber in Fig. 3b, a glass transition occurs at approximately 5.8 °C during the heating process. As the temperature further increases, a distinct endothermic peak appears at 79.2 °C, corresponding to the transition of the material from the liquid crystal phase to the isotropic phase.

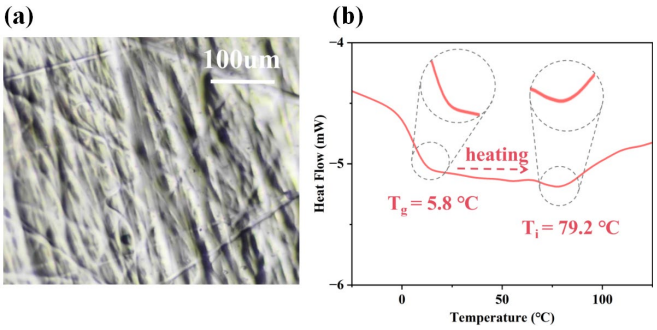

Figure 3. (a) Microstructural image of the composite fiber under optical microscopy. (b) Differential scanning calorimetry (DSC) curve of the composite fiber.

III. RESULT

A. Thermal Actuation Performance

To evaluate the potential of TPU-LCE composite fibers as biomimetic actuators, we systematically characterized their thermal actuation performance. Fig. 4a illustrates the experimental method for testing the thermal actuation performance of fibers under load. Using fibers with a diameter of 0.43 mm, we investigated the contraction-strain relationship of LCE fibers and TPU-LCE composite fibers under different loads (Fig. 4b). The curve for pure LCE fibers is incomplete, as they tend to fracture under relatively high loads (approximately 400 times their own weight) when heated with a hot air gun, indicating their brittle nature at elevated temperatures. In contrast, the curve for TPU-LCE fibers is complete and continuous. Even under high loads where contraction strain decreases, they continue to operate safely without damage. The TPU microdomains significantly enhance the material's toughness and reliability by inhibiting crack propagation and dispersing stress. Uniaxial tensile tests on composite fibers with different TPU contents further validated this conclusion (Fig. 4g). Composite fibers with 16% TPU exhibited superior fracture elongation and tensile strength. However, when the TPU content reached 20%, the fiber elongation decreased. This is attributed to the increased interfacial area between the two phases at high TPU content, which easily becomes stress concentration points during stretching, triggering the initiation and propagation of microcracks.

We also studied the temperature-strain and time-strain relationships of composite fibers with different diameters (Fig. 4c and Fig. 4d), using a uniform heat source of a 270°C hot air gun. During actuation, the surface temperature of the TPU–LCE fiber was monitored in real time using a FOTRIC 616C infrared thermal imaging camera (FOTRIC, China), which offers a thermal sensitivity of <50 mK and a temperature accuracy of ±2 °C or ±2% of the reading. The emissivity was set to 0.93 based on calibration against reference polymer samples with similar surface properties. Thermal images were captured at 25 Hz, and the average temperature over the central

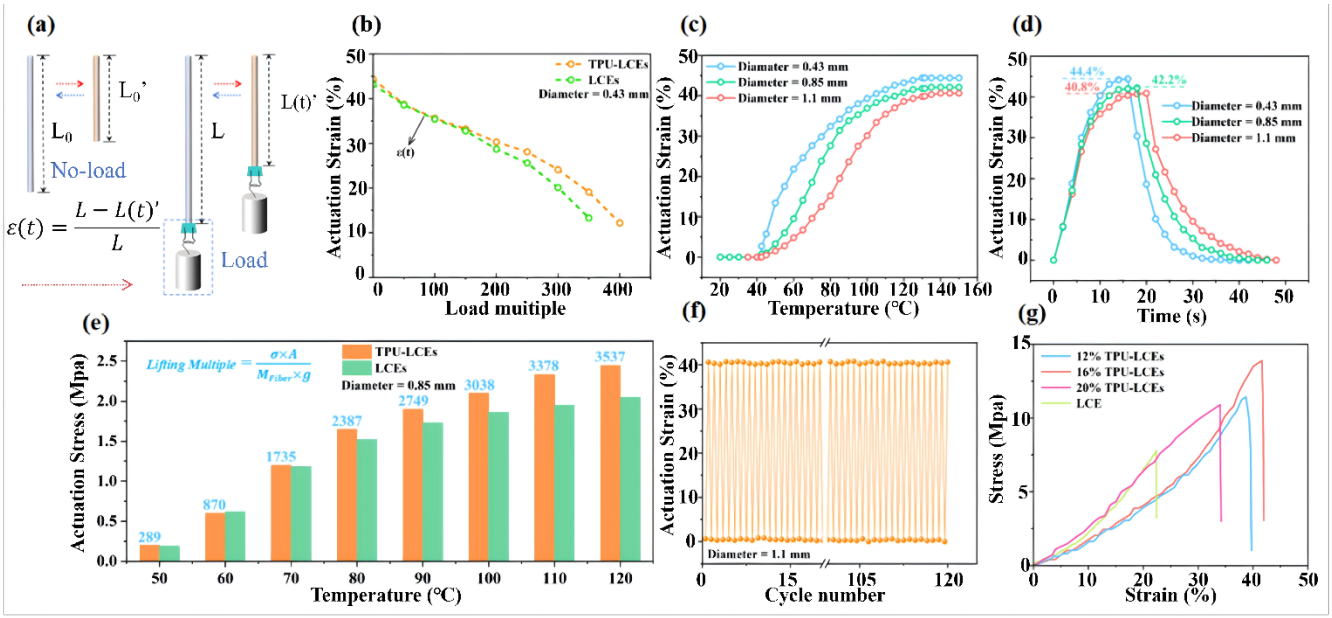

Figure 4. (a) Schematic diagram of the experimental method for measuring the actuation strain of fibers. (b) Relationship curve between the actuation strain of TPU-LCEs fibers and LCEs fibers and their respective load multiples. (c) Relationship between temperature and actuation strain for TPU-LCE fibers with different diameters. (d) Relationship between time and actuation strain for TPU-LCE fibers with different diameters. (e) Bar chart of driving stress of TPU-LCE and LCE at different temperatures and their equivalent self-weight multiples for fiber actuation. (f) Image of 120 thermal actuation cycles of the composite fiber. (g) Uniaxial tensile test curves of composite fibers with different TPU contents.

5 mm segment of the fiber was extracted for correlation with strain measurements. This non-contact approach effectively minimizes interference with the soft actuator's motion while providing spatially resolved thermal data. Thinner fibers exhibit higher thermal sensitivity, enabling completion of heating-cooling cycles within a shorter duration and exhibiting slightly higher maximum contraction strains. The thermal actuation process essentially involves heat transfer from the surface to the interior, inducing LCE phase transition, followed by cooling to dissipate internal heat to the environment. Fiber diameter directly determines the efficiency of this process. Thicker fibers exhibit slower response speeds and slightly lower contraction rates due to their smaller specific surface area and longer thermal conduction paths. This is primarily attributed to the temperature gradients formed within their structure during heating-cooling cycles and their higher heat capacity. This phenomenon highlights the necessary trade-off between response speed and output force in actuator design. As shown in the figures, the axial actuation strain generated by the fibers under thermal stimulation reached up to 44.4%. Compared with various types of soft actuators reported previously, this performance far outperforms the strain upper limit of shape memory alloys (less than 10%) [20]. In contrast, traditional dielectric elastomer actuators rely on a strong voltage (4 kV) [21] to reach this index. This achievement fully demonstrates the deformation amplification effect brought by our composite electrospinning process—its excellent performance is sufficient to enable joint movement in the bionic finger system. This strain originates from the order-disorder transition of mesogens in the LCE component (Fig. 2b): upon heating, the mesogens transition from a highly oriented nematic phase to an isotropic disordered phase, resulting in macroscopic axial contraction. The TPU microdomains form a stable, cross-linked elastic network that effectively anchors the LCE molecular chains, significantly inhibiting creep and ensuring the stability and repeatability of the actuation strain. TPU-LCE composite fibers demonstrated superior mechanical robustness. The incorporation of a TPU framework effectively prevented the brittle fracture and plastic deformation commonly observed in pure LCE during cyclic actuation. Over 120 consecutive thermal actuation cycles, the composite fibers showed no significant performance degradation, exhibiting excellent cyclic stability (Fig. 4f). This confirms that the TPU-reinforced material can effectively suppress the issues of strain accumulation and brittle fracture commonly observed in pure LCE fibers. Although its service life is shorter than that of traditional motor systems, it has laid a solid foundation for subsequent optimization. In the future, by improving the electrospinning parameters and composite material formulations, it is expected that the reliability can be enhanced to the level of tens of thousands of cycles.

Additionally, the actuation stress of the fibers was measured using a mechanical testing setup and further analyzed with infrared imaging, resulting in a bar chart illustrating the relationship between actuation stress and temperature (Fig. 4e). Above 80°C, the actuation stress of the composite fibers was significantly higher than that of pure LCE fibers. Based on formula conversion, the maximum load-bearing capacity exceeded 3,500 times their own weight, exhibit extremely high specific strength, which ensures that these fibers can reliably transmit force in tendon-driven robotic systems even when they bear external stress during grasping movements.

In summary, TPU-LCE composite fibers successfully combine the large actuation strain characteristics of LCE materials with the high toughness of TPU polymers. The composite fibers not only exhibit a contraction strain as high as 44.4%, surpassing common smart material actuators, but

also have a load-bearing capacity reaching 3500 times their own weight, and maintain stable operation without degradation over 120 cycles. While maintaining remarkable thermal actuation performance, they significantly improve mechanical durability, providing a reliable material platform for the development of next-generation soft actuators. reliable material platform for the development of next-generation soft actuators.

B. Actuation of the Biomimetic Finger

To evaluate the actuation performance of TPU-LCE fibersas soft actuators, we designed a biomimetic finger device inspired by the tendon-driven mechanism of the human finger. This device mimics the synergistic action of flexor and extensor tendons in human fingers by deploying TPU-LCE composite fibers as artificial "tendons" on the dorsal and volar sides, respectively, achieving human-like bidirectional actuation. The skeletal structure of the device was fabricated using carbon fiber-reinforced high-temperature nylon material via 3D printing, enabling continuous and stable operation at temperatures up to 150 °C. Two miniature heating elements (1×1 cm each) were integrated on the dorsal and volar sides as compact thermal sources. The TPU-LCE composite fibers were assembled into pre-embedded channels, ensuring tight contact with the heaters for efficient heat transfer.

The dynamic joint angles of the finger served as a key metric for evaluating its biomimetic performance (Fig. 5a). To systematically assess the bio-fluidity of the finger's motion, we recorded its full actuation cycle—"relaxation–extension–flexion" (Fig. 5b). Fig. 5c shows the variation of joint angles over time after power activation:

1) Relaxed state: Before activation, the finger remained in a natural resting posture, with the distal interphalangeal (DIP), proximal interphalangeal (PIP), and metacarpophalangeal (MCP) joint angles measuring 25°, 21°, and 44°, respectively. Both actuation fibers were inactive.

2) Extension motion: When the dorsal heater was activated, the upper fiber contracted under thermal stimulation, mimicking the function of human extensor tendons. This drove coordinated joint movement, transitioning the finger gradually from a relaxed state to full extension.

3) Flexion motion: After deactivating the dorsal heater and activating the volar heater, the lower fiber contracted, simulating human flexor tendons, while the upper fiber relaxed upon cooling. The finger smoothly transitioned from an extended posture to a flexed state.

Experimental results indicated that the joint motion ranges of the biomimetic finger were as follows: DIP: 3–77°, PIP: 6–75°, and MCP: 21–79°. Compared to the typical range of motion of healthy human fingers (DIP: ~0–80°, PIP: ~0–100°, MCP: ~0–90°), the biomimetic finger exhibited close agreement with human performance in DIP and MCP joint mobility. During extension movements, the PIP joint and DIP joint start extending almost simultaneously. Given their similar morphological structures, the two joints exhibit a coupled motion with nearly parallel curve variations, demonstrating a high level of coordination. This ensures the fingertips can smoothly fold toward the palm. In flexion movements, the flexion curves of all joints show a slight S-shape, consisting of an acceleration phase, a constant velocity phase, and a deceleration phase. This indicates that the movement is smooth and well-controlled.

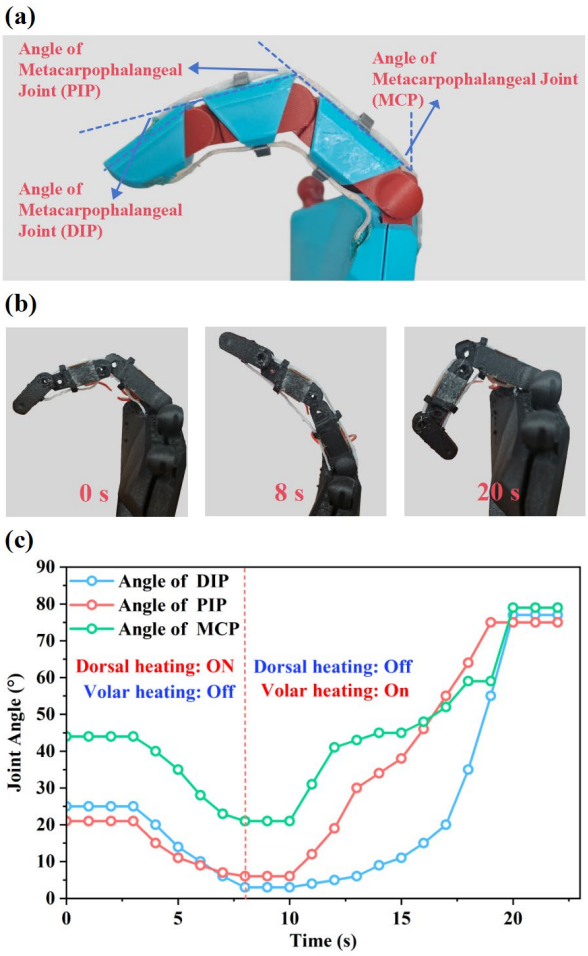

Figure 5. (a) Schematic diagram of joint angles in the biomimetic finger. (b) Sequential motion postures of the biomimetic finger: relaxed, extended, and flexed states. (c) Variation curves of joint angles over time for the biomimetic finger after power activation.

To summarize, the movement of human fingers is not an independent activity of individual joints, but a sophisticated dynamic process in which all joints flex in a coordinated manner according to a specific sequence. The angle-time curves are smooth and continuous, with distinct phase and timing characteristics. A successful bionic finger design must not only replicate the range of motion of human fingers but, more crucially, mimic this inherent dynamic coordination trend to achieve natural and smooth biomechanical performance. It is observed that the range of motion distribution among the joints of the proposed bionic finger differs from that of a natural human hand. Specifically, the DIP joint has the largest range of motion, with the most significant curve variation, contributing to the majority of the movement stroke. This contrasts with the natural finger, where the MCP joint dominates the motion. We analyze that this phenomenon stems from the following reasons: First, the effective moment arm of the driving tendon on the DIP joint is longer. The same contraction force generates a larger driving torque on the DIP joint, thereby amplifying its movement angle. Second, the structural damping of the MCP and PIP joints may be

relatively higher, which dissipates part of the driving energy. As a result, the driving energy is more concentrated on the DIP joint (with the smallest damping) and converted into kinetic energy.

Future work can further adjust the motion distribution ratio among joints by optimizing joint stiffness and tendon routing, to obtain a motion pattern that is either more similar to that of biological fingers or more suitable for specific tasks. This artificial tendon system, inspired by biological tendon actuation mechanisms, offers a novel approach to the bio-inspired design of soft actuators.

IV. Conclusion

Despite the promising actuation performance of the TPU–LCE composite, several limitations should be acknowledged. First, the actuation speed is inherently limited by thermal diffusion and passive cooling, resulting in response cycles on the order of several seconds—significantly slower than electromagnetic or pneumatic alternatives. Future work could integrate rapid heating strategies, such as Joule heating (via conductive fillers) or photothermal excitation, to accelerate thermal cycling. Second, while TPU greatly enhances toughness, processability, and cyclic durability, it inevitably reduces the effective LCE volume fraction, slightly lowering the maximum achievable strain and increasing thermal mass, which modestly slows thermal response. Nevertheless, this trade-off is favorable for tendon-driven applications where reliability and load transmission outweigh peak strain.

The energy required for a single actuation cycle can be estimated based on the heat needed to raise the temperature of the tendon-like fiber bundle (mass: 0.04 g) through its nematic–isotropic transition. Assuming a specific heat capacity of 1.8 J/(g·K) and a temperature increase of approximately 150 K (from ambient to actuation temperature), the theoretical minimum energy input is about 10.8 J per cycle. While this represents only the energy absorbed by the material—and actual consumption using a hot-air gun is significantly higher due to convective losses—it provides a baseline for comparing with alternative heating strategies (e.g., Joule or photothermal actuation) that could improve efficiency and enable portable operation.

This work demonstrated the design and fabrication of a novel soft actuator based on electrospun TPU-LCE composite fibers. By integrating the large actuation strain of LCE (up to 44.4%) with the toughness and elasticity of TPU, the composite fibers effectively overcame the brittleness of pure LCE while maintaining excellent thermal responsiveness. Mechanical tests confirmed superior tensile strength and elongation, while cyclic experiments showed stable performance over 120 consecutive actuation cycles.

Inspired by the tendon-driven mechanism of human fingers, we further implemented the composite fibers in a biomimetic finger device. The artificial tendon system enabled smooth bidirectional motion, with joint ranges (DIP: 3–77°, MCP: 21–79°) closely matching those of human fingers. Moreover, the actuator exhibited an exceptionally high load-bearing capacity exceeding 3,500 times its own weight, highlighting its practical potential for miniaturized robotic applications.

Overall, this study establishes a reliable and scalable strategy for fabricating high-performance TPU-LCE composite fibers via electrospinning. The proposed bioinspired tendon actuator combines high actuation strain, robustness, and durability, offering broad opportunities for the development of next-generation soft robotic systems.

Looking forward, this fiber-based actuation strategy offers a scalable route toward compact and efficient artificial tendons. Future work will focus on incorporating rapid heating methods such as electrical or optical stimuli to enhance response speed, extending the actuation concept to multi-joint or full-hand systems, and exploring multimodal control strategies for programmable soft robotics. Overall, TPU–LCE composite fibers provide a promising material platform for high-performance, bio-inspired tendon actuators.

Acknowledgment

This work was supported by the grants from the National Natural Science Foundation of China (No. 62303290).

References

[1] D. Rus and M. T. Tolley, “Design, fabrication and control of soft robots,” Nature, vol. 521, no. 7553, pp. 467–475, May 2015.

[2] G.-Z. Yang et al., “The grand challenges of Science Robotics,” Sci. Robot., vol. 3, no. 14, p. eaar7650, Jan. 2018.

[3] K. Chubb, D. Berry, and T. Burke, “Towards an ontology for soft robots: what is soft?,” Bioinspir. Biomim., vol. 14, no. 6, p. 063001, Oct. 2019.

[4] S. I. Rich, R. J. Wood, and C. Majidi, “Untethered soft robotics,” Nat Electron, vol. 1, no. 2, pp. 102–112, Feb. 2018.

[5] D. J. Roach et al., “Long Liquid Crystal Elastomer Fibers with Large Reversible Actuation Strains for Smart Textiles and Artificial Muscles,” ACS Appl. Mater. Interfaces, vol. 11, no. 21, pp. 19514–19521, May 2019.

[6] J. M. Boothby, J. C. Gagnon, E. McDowell, T. Van Volkenburg, L. Currano, and Z. Xia, “An Untethered Soft Robot Based on Liquid Crystal Elastomers,” Soft Robotics, vol. 9, no. 1, pp. 154–162, Feb. 2022.

[7] Q. He, Z. Wang, Y. Wang, A. Minori, M. T. Tolley, and S. Cai, “Electrically controlled liquid crystal elastomer–based soft tubular actuator with multimodal actuation,” Sci. Adv., vol. 5, no. 10, p. eaax5746, Oct. 2019.

[8] S. Li et al., “Digital light processing of liquid crystal elastomers for self-sensing artificial muscles,” Sci. Adv., vol. 7, no. 30, p. eabg3677, July 2021.

[9] S. W. Ula, N. A. Traugutt, R. H. Volpe, R. R. Patel, K. Yu, and C. M. Yakacki, “Liquid crystal elastomers: an introduction and review of emerging technologies,” Liquid Crystals Reviews, vol. 6, no. 1, pp. 78–107, Jan. 2018.

[10] K. M. Herbert, H. E. Fowler, J. M. McCracken, K. R. Schlafmann, J. A. Koch, and T. J. White, “Synthesis and alignment of liquid crystalline elastomers,” Nat Rev Mater, vol. 7, no. 1, pp. 23–38, Sept. 2021.

[11] M. Chen, M. Gao, L. Bai, H. Zheng, H. J. Qi, and K. Zhou, “Recent Advances in 4D Printing of Liquid Crystal Elastomers,” Advanced Materials, vol. 35, no. 23, p. 2209566, June 2023.

[12] W. Hou, J. Wang, and J. Lv, “Bioinspired Liquid Crystalline Spinning Enables Scalable Fabrication of High-Performing Fibrous Artificial Muscles,” Advanced Materials, vol. 35, no. 16, p. 2211800, Apr. 2023.

[13] Y. Wang et al., “Liquid Crystal Elastomer Based Dexterous Artificial Motor Unit,” Advanced Materials, vol. 35, no. 17, p. 2211283, Apr. 2023.

[14] M. Zadan et al., “Liquid Crystal Elastomer with Integrated Soft Thermoelectrics for Shape Memory Actuation and Energy

Harvesting," Advanced Materials, vol. 34, no. 23, p. 2200857, June 2022
[15] H. Yang et al., "Fabrication and Photothermal Actuation Performances of Electrospun Carbon Nanotube/Liquid Crystal Elastomer Blend Yarn Actuators," ACS Appl. Mater. Interfaces, vol. 16, no. 7, pp. 9313–9322, Feb. 2024.
[16] J. Ma and Z. Yang, "Smart liquid crystal elastomer fibers," Matter, vol. 8, no. 2, p. 101950, Feb. 2025.
[17] J. Liu, Y. Gao, H. Wang, R. Poling-Skutvik, C. O. Osuji, and S. Yang, "Shaping and Locomotion of Soft Robots Using Filament Actuators Made from Liquid Crystal Elastomer–Carbon Nanotube Composites," Advanced Intelligent Systems, vol. 2, no. 6, p. 1900163, June 2020.
[18] X. Liu, X. Zhou, and Z. Liu, "Strengthening Liquid Crystal Elastomer Muscles," Acc. Chem. Res., vol. 58, no. 6, pp. 907–918, Mar. 2025.
[19] J. Küpfer and H. Finkelmann, "Nematic liquid single crystal elastomers," Makromol. Chem., Rapid Commun., vol. 12, no. 12, pp. 717–726, Dec. 1991.
[20] W. Gao, X. Yi, G. Song, Z. Wang, and X. Meng, "Zr50Cu25Ni7.5Co17.5 high-temperature shape memory alloy with excellent thermal stability and large recovery strain, and the associated microstructural deformation mechanism," Materials & Design, vol. 196, p. 109108, Nov. 2020.
[21] Y. Shi et al., "A processable, high-performance dielectric elastomer and multilayering process," Science, vol. 377, no. 6602, pp. 228–232, July 2022.